Neuron
Article

Multiplexing of Motor Information in the Discharge of a Collision Detecting Neuron during Escape Behaviors

Haleh Fotowat,[1,5,*] Reid R. Harrison,[2,3,6] and Fabrizio Gabbiani[1,4,*]
[1]Department of Neuroscience, Baylor College of Medicine, Houston, TX 77030, USA
[2]Department of Electrical and Computer Engineering
[3]Department of Biomedical Engineering
University of Utah, Salt Lake City, UT, 84112, USA
[4]Computational and Applied Mathematics, Rice University, Houston, TX 77005, USA
[5]Present address: Department of Biology, McGill University, Montreal, Quebec H3A-1B1, Canada
[6]Present address: Intan Technologies, LLC, 8726 S. Sepulveda Boulevard., Suite D2121, Los Angeles, CA 90045, USA
*Correspondence: haleh.fotowat@mail.mcgill.ca (H.F.), gabbiani@bcm.edu (F.G.)
DOI 10.1016/j.neuron.2010.12.007

SUMMARY

Locusts possess an identified neuron, the descending contralateral movement detector (DCMD), conveying visual information about impending collision from the brain to thoracic motor centers. We built a telemetry system to simultaneously record, in freely behaving animals, the activity of the DCMD and of motoneurons involved in jump execution. Cocontraction of antagonistic leg muscles, a required preparatory phase, was triggered after the DCMD firing rate crossed a threshold. Thereafter, the number of DCMD spikes predicted precisely motoneuron activity and jump occurrence. Additionally, the time of DCMD peak firing rate predicted that of jump. Ablation experiments suggest that the DCMD, together with a nearly identical ipsilateral descending neuron, is responsible for the timely execution of the escape. Thus, three distinct features that are multiplexed in a single neuron's sensory response to impending collision—firing rate threshold, peak firing time, and spike count—probably control three distinct motor aspects of escape behaviors.

INTRODUCTION

The transformation of sensory signals into motor commands plays a pivotal role in the generation of behavior. Much work, both in vertebrates and invertebrates, has focused on characterizing how the spike trains of sensory neurons may determine the motor output of an organism (Mountcastle et al., 1975; Newsome et al., 1988; Trimarchi and Schneiderman, 1993; Lewis and Kristan, 1998; Edwards et al., 1999; van Hateren et al., 2005; Santer et al., 2006; Marsat and Pollack, 2006; Lima and Miesenböck, 2005; Korn and Faber, 2005; Ishikane et al., 2005; De Lafuente and Romo, 2005; Gu et al., 2008; Cohen and Newsome, 2009; Nienborg and Cumming, 2009). In particular, both the mean number of spikes, and firing rate thresholds in sensory neuron populations have been implicated (Camhi and Levy, 1989; Cook and Maunsell, 2002; Roitman and Shadlen, 2002). Yet, little is known about how the time-varying firing rate of sensory neurons control the specific motor sequences underlying ongoing, complex motor behaviors.

Collision avoidance and escape behaviors provide a favorable model to study this question. They are critical for survival and are implemented by specialized neural circuits in several species (Wang and Frost, 1992; Graziano et al., 1994; Wicklein and Strausfeld, 2000; Yamamoto et al., 2003; Preuss et al., 2006; Oliva et al., 2007; Fotowat et al., 2009). In locusts, the third neuropil in each of the two optic lobes contains an identified neuron, the lobula giant movement detector (LGMD) that responds specifically to objects approaching on a collision course in its associated visual hemifield, or their 2D projection: looming stimuli (Hatsopoulos et al., 1995; Schlotterer, 1977; Rind and Simmons, 1992; Judge and Rind, 1997; Peron and Gabbiani, 2009). Each LGMD synapses in the brain onto the descending contralateral movement detector (DCMD) neuron, such that their spikes are in one-to-one correspondence (Rind, 1984; Killmann and Schurmann, 1985). In response to looming stimuli, the firing rate of these neurons gradually increases, peaks, and rapidly decreases before expected collision (Gabbiani et al., 1999). Similar response profiles have now been described in neurons of wide-ranging species (pigeon: Sun and Frost, 1998; frog: Nakagawa and Hongjian, 2010; fish: Preuss et al., 2006; fruit fly: Fotowat et al., 2009). In locusts, this response profile is robust to a broad spectrum of stimulus changes, suggesting that it may play an important role in the generation of escape behaviors (Gabbiani et al., 2001).

From the brain, each DCMD axon projects through the contralateral nerve cord to motor centers involved in jump and flight steering (O'Shea et al., 1974; Simmons, 1980). In particular, the DCMDs make both direct and indirect synaptic contacts with the fast extensor tibia (FETi) motoneuron of the hindleg and indirect connections to the flexor tibia motoneurons (Burrows and Rowell, 1973; Pearson et al., 1980; Pearson and Robertson, 1981).

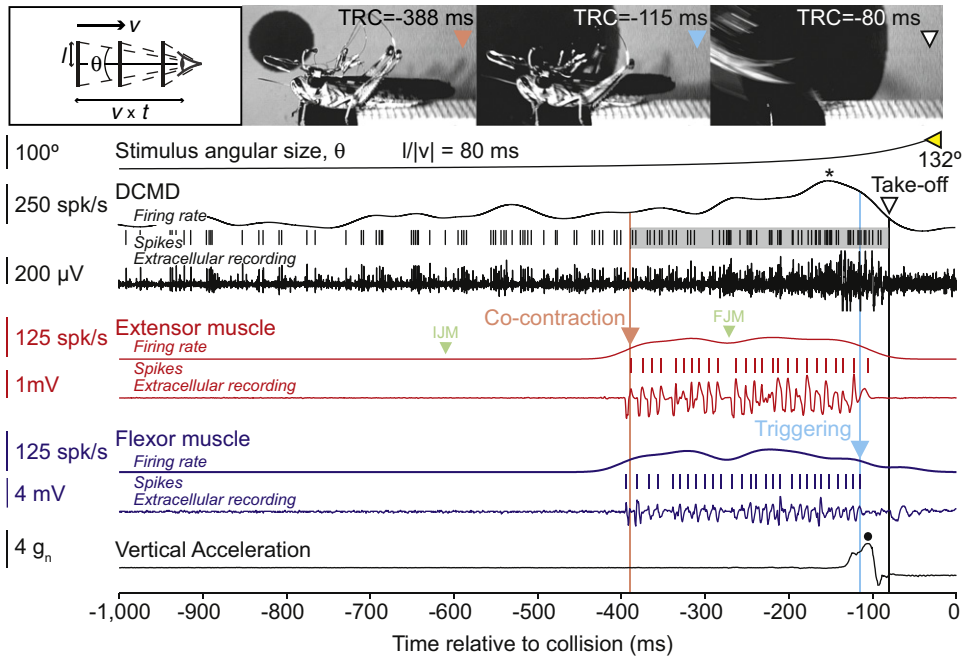

Figure 1. Neural, Muscle, and Acceleration Recordings Obtained during Jump Behavior with Wireless Telemetry

Time markers and corresponding video frames for the onset of cocontraction, its end (triggering), and take-off are indicated with ▼, ▼, and ▽, respectively; ◂ marks the final angular size (see also Movie S1). The timing of the IJM and FJM are marked by the symbols [•] (see Results). Cocontraction starts before, and take-off occurs after, the peak (*) DCMD firing rate (TRC is used as an abbreviation for time relative to collision). The shaded area around the DCMD spikes corresponds to the time period over which they were counted for further analysis (see Results). The right and left bounds of the shaded area are the cocontraction onset and take-off time, respectively. Peak vertical acceleration is marked by a ●. Top left inset: Schematics of the stimuli. Discs of radius l approaching at constant speed v subtend an angle θ at the retina. By convention $v < 0$ for approaching objects and $t < 0$ before collision (bottom axis); $v \times t$ is the distance of the object to the eye.

The involvement of DCMD activity in jump escape behaviors has been studied, but its role remains unclear (Fotowat and Gabbiani, 2007; Burrows, 1996; Santer et al., 2005). Up to now, it was impossible to record simultaneously from the DCMD and motoneurons during freely executed, visually guided jump escape behaviors. Consequently, it was not possible to observe how sensory and motor activities are related on a trial-by-trial basis. To achieve this goal, we built a telemetry system capable of wireless transmission of neural and muscle recordings. This system was sufficiently small that locusts could carry it as a backpack and still respond to looming stimuli by jumping. We also developed a technique allowing us to selectively laser ablate the DCMD before behavioral jump experiments to further assess the relationship between its neural activity and escape behaviors.

RESULTS

Our digital telemetry system allowed us to monitor simultaneously the sensory and motor activity evoked by looming stimuli during collision avoidance behaviors (Experimental Procedures and Figure S1, available online). The simulated objects were black discs on a bright background with various size to speed ratios, $l/|v|$, where l is the disc radius and $|v|$ the approach speed. This parameter has units of time and determines the stimulus angular size, $\theta(t)$, since by trigonometry the tangent of $\theta/2$ is the ratio of l to the object's distance ($v \times t$; Figure 1, Experimental Procedures). Equivalently, $l/|v|$ is the time remaining to collision when the stimulus subtends 90° on the retina. Thus, the faster the stimulus approach speed, $|v|$, the smaller $l/|v|$. Looming stimuli were always presented on one side of the animal so that a single DCMD neuron was stimulated.

Energy Storage Starts before, and Take-Off Occurs after Peak DCMD Firing Rate

Figure 1 shows a trial in which a locust jumped in response to a looming stimulus (Movie S1). Spikes from the DCMD, the FETi, and flexor motoneurons were obtained by extracellular recording from the contralateral nerve cord, the hindleg extensor, and flexor muscles, respectively. The time course of vertical acceleration was measured by an on-board accelerometer. The locust jump is a complex behavior, consisting of several distinct phases, during which the animal orients itself away from the approaching object using its middle legs and stores the energy required for take-off in the elastic elements of its hindlegs (Burrows, 1996; Santer et al., 2005). By monitoring the position of the hindleg femur-tibia joint, we previously showed that after an initial flexion of the tibia, the joint moves to align the leg parallel to the body (initial joint movement [IJM]; Fotowat and Gabbiani, 2007). Subsequently, the flexor and extensor muscles contract simultaneously to store the mechanical energy required for the jump (cocontraction). This leads to a final femur-tibia joint

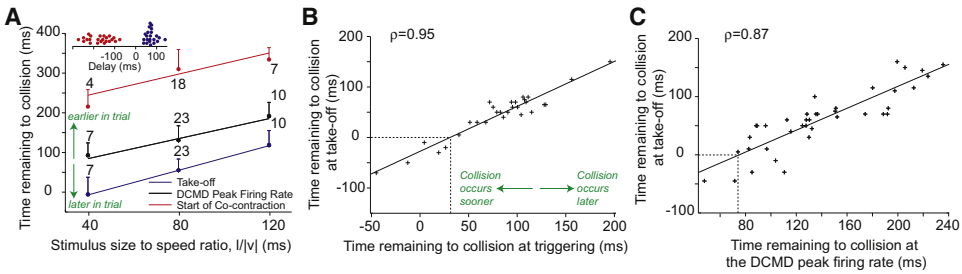

Figure 2. Relative Timing of Jump-Escape Stages in Freely Behaving Animals

(A) Timing of cocontraction onset (red), DCMD peak firing rate (black), and take-off (blue) in response to looming stimuli with l/|v| = 40, 80, and 120 ms (mean and SD; n_T shown on figure). The timing of these stages was highly correlated with l/|v|, $\rho = 0.57$, 0.69, and 0.78, respectively. Slopes (α) and intercepts (δ) of linear fits were as follows. Start of cocontraction: $\alpha = 1.33$ (SD: 0.37), $\delta = 191$ ms (SD: 33); DCMD peak: $\alpha = 1.26$ (SD: 0.22), $\delta = 34$ ms (SD: 19); Take-off: $\alpha = 1.55$ (SD: 0.20), $\delta = -69$ms (SD: 18). Top inset: Representative delays between DCMD peak and cocontraction onset (red) and between peak and take-off (blue; $n_T = 23$). Positive delays correspond to events after the peak (data points staggered vertically for clarity).

(B) The end of cocontraction (triggering) and take-off were highly correlated ($\rho = 0.95$, data pooled across l/|v| values). Linear fit slope: 0.89 (SD: 0.06); intercept: −27 ms (SD: 3.7), indicating that take-off occurs approximately 27 ms after triggering (dashed line).

(C) Timing of DCMD peak firing rate and take-off relative to expected collision time were highly correlated ($\rho = 0.87$, data pooled across l/|v| values). Linear fit slope: 0.94 (SD: 0.09); intercept: −70 ms (SD: 13), indicating that take-off occurs approximately 70 ms after the DCMD peak (dashed line). $n_L = 9$ for DCMD and take-off data, $n_L = 4$ for cocontraction data.

movement (FJM), which is followed by cessation of activity in the flexors (triggering) that allows energy release and take-off. Looming stimuli with l/|v| values larger than 40 ms led to jumps before the expected collision time. As illustrated in Figure 1, locusts started to accelerate toward the end of cocontraction, and vertical acceleration peaked immediately after triggering (mean: 5.8 g_n, standard deviation [SD]: 1.3; number of locusts, $n_L = 3$, number of trials, $n_T = 20$; Experimental Procedures). During cocontraction, the flexors and extensors fired fairly regular spike trains (mean ISI: 14 ms, CV: 0.69, $n_L = 4$, $n_T = 54$), and the number of their spikes were highly correlated ($\rho = 0.8$, $p < 10^{-9}$). The DCMD firing rate gradually increased, peaked, and sharply decreased before projected collision, as observed in fixed animals (Fotowat and Gabbiani, 2007). Figure 1 shows that the cocontraction phase started before the DCMD firing rate reached its peak (mean: 169 ms, SD: 49, $n_L = 3$, $n_T = 24$), whereas take-off occurred afterward. This was the case in every trial for all animals (Figure 2A).

Which aspects of the motor and sensory activity determine the timing of the jump? We found that the time at which the cocontraction ended (triggering) was highly correlated with take-off ($\rho = 0.95$, $p < 10^{-9}$). Moreover, this correlation exists regardless of l/|v|, since the partial correlation coefficient between these two variables controlling for l/|v| remained high ($\rho_{part} = 0.94$, $p < 10^{-9}$). On average take-off occurred 36 ms after triggering (SD: 15, $n_L = 4$, $n_T = 29$; Figure 2B, dashed line) and 90% of the variance in the timing of take-off could be explained by the timing of triggering. At the sensory level, we found that the timing of the DCMD peak firing rate and take-off were highly correlated as well ($\rho = 0.87$, $p < 10^{-9}$) and that the partial correlation coefficient between these variables controlling for l/|v| also remained high ($\rho_{part} = 0.73$, $p = 9.2 \times 10^{-8}$). Locusts took off on average 70 ms (SD: 13) after the DCMD firing rate peaked, regardless of l/|v| (Figure 2C, dashed line) and the timing of the peak accounted for 75% of the variance of the take-off time.

Comparison of Sensory-Motor Activity in Trials with and without Jump

Not all looming stimuli led to a final take-off. Thus, locusts jumped with a median probability of 32%. The jump probability was significantly reduced compared to that of animals without a telemetry backpack (Fotowat and Gabbiani, 2007; median: 64%, $p_{KWT} = 0.003$). Figure 3 shows a trial in which the same locust as in Figure 1 did not jump (Movie S2). It started preparing by cocontracting its hindleg flexor and extensor muscles. However, compared to jump trials, the cocontraction started late, such that after a few spikes in the extensor, the looming stimulus reached its full size, the DCMD firing rate declined, and the cocontraction ended. This was the case in 85% of trials without take-off, whereas in the remaining 15% the cocontraction failed to initiate altogether.

Across animals, we found that cocontraction onset occurred significantly earlier relative to collision in jump trials (Figure 4A), whereas the timing of the DCMD peak itself did not change (Figure 4B). Thus, while the DCMD peak time predicts the time of take-off, it fails to predict its occurrence. Since cocontraction started earlier in jump trials, the number of extensor spikes was also significantly higher (Figure 4C). In contrast, there was no difference in the total number of DCMD spikes between jump and no-jump trials (Figure 4D), although the peak DCMD firing rate was higher in jump trials (Figure S2A). However, we found that if we started counting the DCMD spikes from cocontraction onset rather than stimulus onset (shaded areas in Figures 1 and 3), their number was significantly higher in jump trials (Figure 4E). Furthermore, the number of DCMD spikes from cocontraction onset was highly correlated with the number of extensor spikes ($\rho = 0.73$, $p < 10^{-9}$, Figure 4F), such that on average 4.3 DCMD spikes led to one extensor spike (SD: 2.1 spikes). To further test for a possible causal relation between the DCMD and extensor firing rates following cocontraction onset, we designed looming stimuli that abruptly stopped in midcourse and resumed

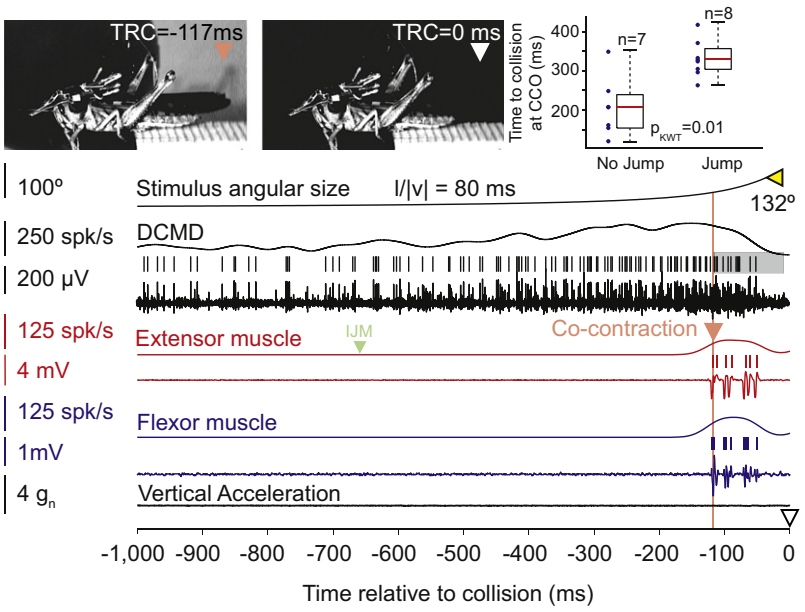

Figure 3. Neural and Muscle Recordings during a Trial in which the Animal Did Not Take Off

The symbols ▼ and ▽ mark the start of cocontraction and the expected collision time, respectively (and corresponding video frames in Movie S2); ◁ marks the final angular size (see also Movie S2). The locust prepares to jump by cocontracting its flexor and extensor muscles but never takes off (same animal as in Figure 1). The shaded area around the DCMD spikes corresponds to the time period over which they were counted for further analysis (see Results). The right and left bounds are the cocontraction onset and the time at which the DCMD firing rate falls below 5 spk/s, respectively. Top right: Cocontraction onset (CCO) occurred significantly earlier for jumps (all trials at l/|v| = 80 ms, same locust as in main panel). Individual trial values shown on left (dots); corresponding box plots on right (box plot conventions in this and subsequent figures defined in Data Analysis).

their looming immediately thereafter. This often caused the DCMD firing rate to peak twice: once before and once after the abrupt motion cessation (in 13 out of 17 trials, n_L = 3). Under these conditions, the firing rate in the extensor faithfully tracked that of the DCMD in 10 of these 13 trials (Figure S2B). Of the remaining three trials, two failed to elicit extensor spikes, while the last one elicited spikes only after the second DCMD peak.

Which motor or sensory attribute best predicts the occurrence of a jump? To address this question, we trained a naive Bayes classifier to discriminate between jump and no-jump trials based on various sensory and motor attributes (Figure 5). The number of extensor spikes predicted the occurrence of a jump with an accuracy of 70% (SD: 7%). The time of cocontraction onset did even better (83%, SD: 4%). On the sensory side, the number of DCMD spikes after cocontraction onset had a similar accuracy (82%, SD: 6%). In contrast, DCMD attributes computed before cocontraction onset consistently performed poorly. Although several other attributes predicted the occurrence of a jump, none did as well as the time of cocontraction onset or the number of DCMD spikes after cocontraction onset. In particular, the variability of the DCMD spike train, as embodied by the standard deviation of its interspike interval (ISI) distribution, could predict a substantial fraction of the jumps, but it did not improve the prediction accuracy given by the number of DCMD spikes after cocontraction onset. On the other hand, adding information about the mean or SD of the DCMD ISI to the number of extensor spikes significantly improved the performance of the classifier (Figure 2C, attributes 7 and 8). As we explain in the Supplemental Text and Figure S3, it is therefore likely that the increase in the number of DCMD spikes (and a concurrent decrease in the mean and SD of the ISI) results in better summation of these spikes in the FETi and other thoracic interneurons.

Cocontraction Is Triggered a Fixed Delay after a Threshold DCMD Firing Rate

Both the timing of cocontraction (Figure 2A), and a threshold in the DCMD firing rate vary linearly with l/|v| (Gabbiani et al., 2002). We therefore investigated whether a threshold in the DCMD firing rate could play a role in triggering the cocontraction using three different approaches. First, we presented locusts with looming stimuli stopping at various final sizes. Stopping the stimulus at smaller final sizes allowed us to reduce excitation to the DCMD before it peaks and therefore manipulate its maximum firing rate (Gabbiani et al., 2005). Figure 6A shows the DCMD and extensor muscle activity evoked in response to such stimuli. At the lowest final size no extensor spikes were recorded. Increasingly larger final sizes caused a concurrent increase in the DCMD maximal firing rate and the number of extensor spikes. While final angular size was not always a strong predictor of the occurrence of cocontraction (Figures S4A and S4B), the probability distribution of the DCMD maximum firing rate for trials with cocontraction was shifted to larger firing rates compared to trials without cocontraction (Figure 6B). Using a linear discriminant, we could predict with an accuracy of 83% the occurrence of cocontraction based on whether the maximum DCMD firing rate exceeded 248 spike [spk]/s (Figure S4C). Second, in a subset of these trials (n_T = 9, n_L = 6) only one or two extensor spikes were recorded after the stimulus had stopped and the DCMD had reached its maximum activity (Figure S4D). Thus, the maximum DCMD activity in these trials, 300 spk/s on average, was just above the threshold required to trigger the cocontraction (SD: 72). This value is close to that suggested to trigger collision avoidance in flight (Santer et al., 2006) and not significantly higher than that estimated with a linear discriminant (t test, p = 0.073). Furthermore, in these trials the average delay between the maximum DCMD firing rate and the start cocontraction was 36 ms (SD: 23).

As a third approach for assessing the role of a DCMD firing rate threshold in triggering cocontraction, we carried out a correlation analysis on the data recorded in trials with full stimulus expansion. We hypothesized that if the cocontraction is triggered when a fixed delay has elapsed following a threshold DCMD

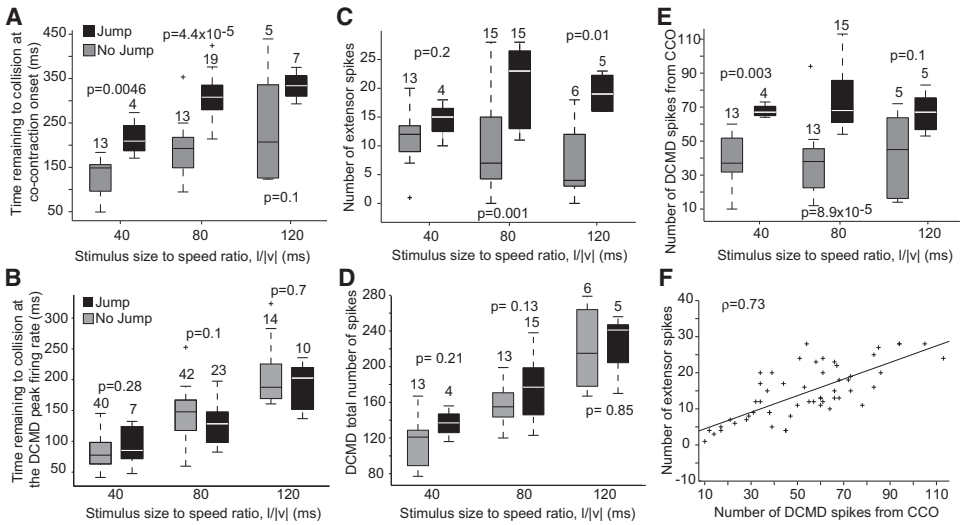

Figure 4. Comparison between Sensory and Motor Activity in Jump and No Jump Trials

(A) Cocontraction started earlier in jump (J) trials (see also Figure S2).

(B) Timing of the DCMD peak rate was not significantly different in J and no-jump (NJ) trials.

(C) The number of extensor spikes was higher and did not change significantly with l/|v| ($p_{KWT\text{-}J}$ = 0.18, $p_{KWT\text{-}NJ}$ = 0.15).

(D) The total number of DCMD spikes was not significantly different in J and NJ trials.

(E) The number of DCMD spikes from CCO was higher in J trials and did not change significantly with l/|v| ($p_{KWT\text{-}J}$ = 0.6, $p_{KWT\text{-}NJ}$ = 0.9).

(F) In both J and NJ trials the number of extensor spikes from CCO was positively correlated with the number of DCMD spikes (linear fit slope: 0.2, SD: 0.09; intercept: 2 spikes, SD: 1.5). KWT p values and n_T shown next to box plots.

Data from four locusts (except [B], where n_L = 10).

firing rate, the value of the firing rate at that delay must be independent of l/|v|. Consistent with this hypothesis, the DCMD firing rate and the stimulus size to speed ratio were uncorrelated 40 ms prior to cocontraction onset (Figure 6C). The firing rate at this delay did not significantly change with l/|v| (p_{KWT} = 0.6) and had an average of 225 spk/s (SD: 73; Figure 6D), close to the values predicted by the two other methods considered above. Taking into account the observed variability, we conclude that the cocontraction is triggered approximately 40 ms after the DCMD approximately exceeds a firing rate of 250 spk/s.

Using data from the same experiments, we next checked that the total number of DCMD spikes from trial start to cocontraction onset was only weakly correlated with the time of cocontraction (ρ = 0.07, p = 0.6). This result is also consistent with a change in DCMD firing rate immediately before cocontraction onset, such as a firing rate threshold, being more critical than accumulation

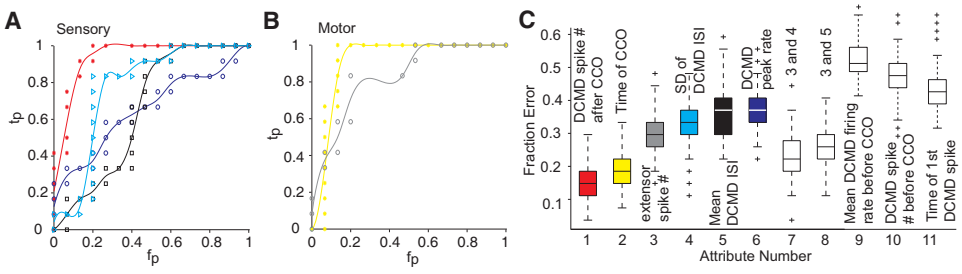

Figure 5. Predicting Take-Off from Sensory and Motor Attributes (see also Figure S3)

(A) Receiver operating characteristics (ROC) curve for naive Bayes classifiers trained to distinguish between J and NJ trials based on the number of DCMD spikes (red), the SD of the DCMD ISI (cyan), the mean DCMD ISI (black), and the DCMD peak firing rate (blue). The following abbreviations are used: t_p, true positives; f_p, false positives.

(B) ROC curve for classifiers trained with the timing of cocontraction onset (CCO, yellow) and the number (#) of extensor spikes (gray).

(C) Misclassification rate of different classifiers trained and tested with 100 random data shuffles (box plots; chance level: 0.5). Attributes are as follows (including medians in J and NJ trials and significance level of their difference). (1) Number of DCMD spikes from CCO (J: 67, NJ: 38, p_{KWT}: 9.4×10^{-8}); (2) Time of CCO relative to projected collision (J: 307 ms, NJ: 152 ms, p_{KWT}: 4.4×10^{-7}); (3) Number of extensor spikes (J: 20, NJ: 10, p_{KWT}: 3.2×10^{-5}); (4) SD of DCMD ISI after CCO (J: 2 ms, NJ: 3 ms, p_{KWT}: 0.0141); (5) Mean DCMD ISI after CCO (J: 3 ms, NJ: 4 ms, p_{KWT}: 4.0×10^{-3}); (6) DCMD peak firing rate (J: 427 spk/s, NJ: 362 spk/s, p_{KWT}: 1.9×10^{-3}); (9) Mean DCMD firing rate before CCO (J: 34 spk/s, NJ: 32 spk/s, p_{KWT}: 0.74); (10) number of DCMD spikes before CCO (J: 112, NJ: 105, p_{KWT}: 0.15); (11) Time of first DCMD spike from stimulus onset (J: 3923 ms, NJ: 3564 ms, p_{KWT}: 0.06).

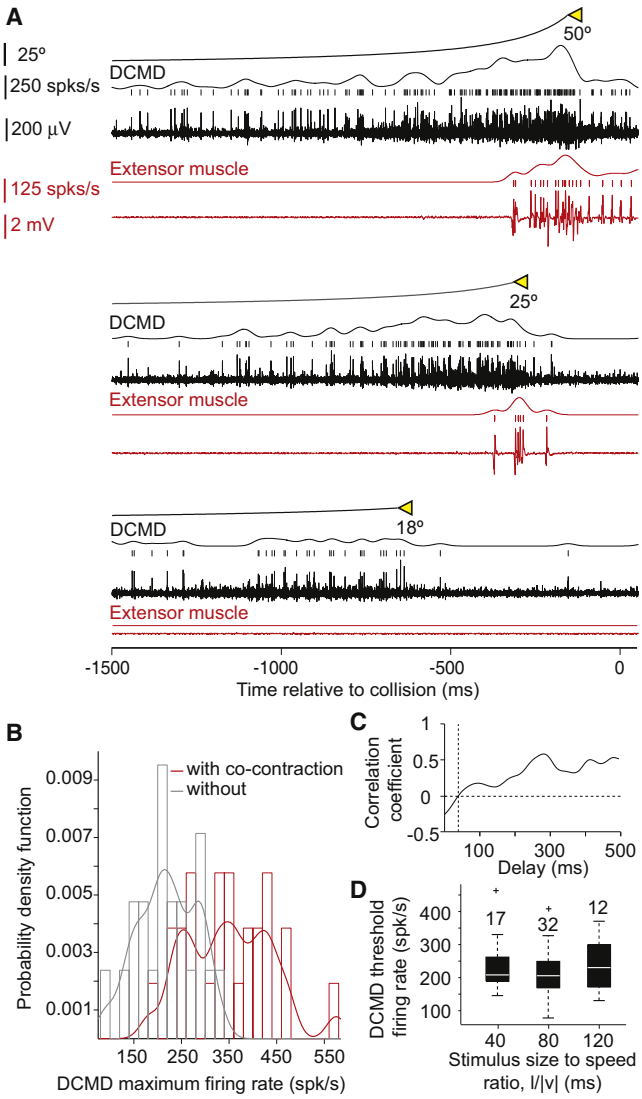

Figure 6. A DCMD Firing Rate Threshold Contributes to Triggering Cocontraction

(A) Example of neural and muscle recordings in response to looming stimuli with three final angular sizes (from bottom to top: 18°, 25°, and 50°; l/|v| = 80 ms). As the final size increases the DCMD maximum firing rate and the total number of extensor spikes increase as well. Cocontraction did not occur for a final size of 18°.

(B) Probability density function (PDF) for the DCMD maximum firing rate in trials with and without cocontraction (red and gray, respectively). The PDF is estimated with a nonparametric fit to the firing rate histogram as the sum of Gaussian kernels with bandwidths equal to 20 spk/s.

(C) Correlation coefficient between DCMD firing rate and l/|v| plotted as a function of delay before cocontraction onset. The correlation coefficient equals zero 40 ms before cocontraction onset.

(D) At that time, the DCMD firing rate does not depend on l/|v| (p_{KWT} = 0.6) and has an average value of 225 spk/s (SD: 73). Box plots of data from four locusts presented with full-expansion looming stimuli.

See also Figure S4.

of spikes over the entire trial. The trial-by-trial correlation of the firing rate threshold time with that of cocontraction onset was high ($\rho = 0.6$, $p < 10^{-9}$; Figure S4E) and predicted 36% of the variance of cocontraction onset. Furthermore, this correlation value decreased by 1/3 when we randomly shuffled these two variables across trials ($\rho = 0.39$, $p = 0.01$; mean over 100 shuffles, SD: 0.07) and was significantly smaller than that obtained without shuffling ($p = 0.001$, Z test). These results also suggest that a DCMD firing rate threshold plays a trial-by-trial role in determining the onset of cocontraction but that other neurons may contribute as well.

To quantify the steepness of the threshold, we plotted the extensor firing rate as a function of the DCMD firing rate and computed the DCMD firing rate change resulting in the extensor sweeping from 5% to 25% of its peak rate (Figure S4F). On average the corresponding relative DCMD firing rate change amounted to ~5% and was thus approximately four times steeper than that of the extensor (20%).

Is the DCMD Activity Necessary for Looming-Evoked Escape Behaviors?

So far, the results suggest that the DCMD strongly contributes to the execution of various phases of looming-evoked escape behaviors. We next asked: Is the DCMD activity *necessary* for their generation? To address this question, we sectioned one of the two nerve cords ($n_L = 6$) and presented looming stimuli to the eye ipsi- or contralateral to the intact nerve cord. We compared the timing and probability of take-off before and after this procedure. We found that, irrespective of the stimulated eye, these locusts still took off and that the timing of take-off remained as positively correlated with l/|v| as in control experiments ($\rho = 0.9$, $p < 10^{-9}$). Moreover, the take-off time was not significantly different when the stimulus was presented to the eye ipsi- or contralateral to the remaining nerve cord (Figure 7A) and was significantly delayed only for l/|v| = 40 ms (Figure 7B; a similar result was obtained at l/|v| = 30 ms, data not shown). The variability in the take-off time was however increased, as reported previously for the time of the initial flexion in tethered locusts (Santer et al., 2008). Additionally, the probability of take-off was reduced on average by 51% (SD: 24%) for stimulation of the eye ipsilateral to the intact cord and 64% (SD: 27%) for stimulation of the contralateral eye. These reductions were not significantly different from each other ($p_{KWT} = 0.42$).

Since locusts with a nerve cord sectioned contralateral to the stimulated eye jump at the same time as control animals, there must exist at least one looming sensitive neuron in the ipsilateral nerve cord whose activity is functionally equivalent to that of the DCMD. This neuron may be the descending *ipsilateral* movement detector neuron (DIMD), which responds to the motion of small targets similarly to the DCMD (Rowell, 1971; Burrows and Rowell, 1973). The DIMD has not been identified anatomically but is known to generate spikes that in some animals are in one-to-one correspondence with those of the DCMD. Furthermore, based on electrophysiological recordings, it is thought to make a monosynaptic connection with the FETi, whose EPSPs summate with those induced by the DCMD. The DIMD is therefore a strong candidate for a mirror symmetric neuron with an equivalent role in generating escape behaviors. Since the response properties of the DIMD to looming stimuli had not yet been characterized, we obtained extracellular recordings simultaneously from both nerve cords in response to the presentation

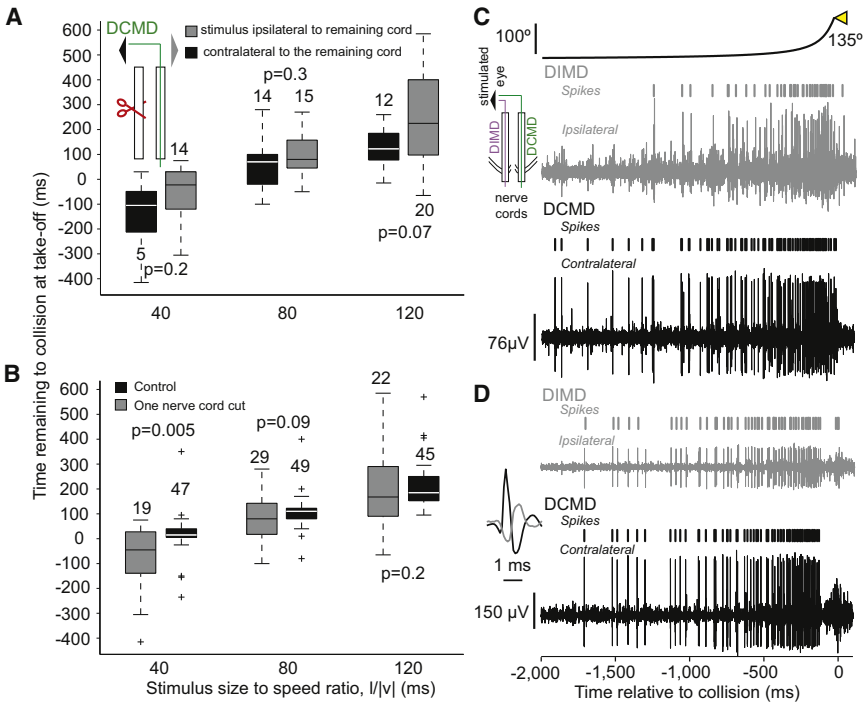

Figure 7. Locusts with One Nerve Cord Sectioned Still Jump in Response to Looming Stimuli and Comparison between Looming-Evoked Activities in the DCMD and DIMD

(A) In animals with one sectioned nerve cord, no significant difference in the timing of take-off was observed, irrespective of the stimulated eye (box plots; $n_L = 6$). Inset: stimulated eye and sectioning procedure (red scissors).

(B) The timing of take-off was significantly delayed at l/|v| = 40 ms relative to control. The timing of take-off showed higher variability after cutting one nerve cord. Box plots of data pooled across trials where the stimulus was presented to the eye ipsi- and contralateral to the remaining nerve cord, since those take-off times did not show a significant difference (A).

(C) Looming-evoked activities in the DCMD and DIMD obtained by simultaneous recording from both nerve cords (inset). In this locust, the DCMD and DIMD spikes were not always coincident.

(D) Recording from a different locust in which the DCMD and DIMD spikes were coincident. Inset: example of coincident DIMD (gray) and DCMD spikes on an expanded time scale. The ipsi- and contralateral extracellular recordings are plotted on the same vertical scale.

See also Figure S5.

of looming stimuli with various l/|v| values to either eye. We found that the DIMD shows a nearly identical activity profile to the DCMD (Figures 7C and 7D). There was no significant difference in the amplitude of the peak firing rate between the two neurons (Figure S5A) except at l/|v| = 10 ms. The DCMD peak firing rate, however, occurred slightly earlier than the DIMD for small l/|v| values (Figure S5B).

The simplest explanation for these results is that the DCMD and the DIMD—given its close resemblance to the DCMD—can interchangeably and equally well mediate jump escape behaviors. According to this hypothesis, because EPSPs elicited in the FETi by these neurons summate, the reduction in jump probability and the increase in variability following nerve cord sectioning would be at least partially explained by the absence of one of them, resulting in delayed cocontraction and a smaller number of subsequent extensor spikes. We conclude that the DCMD is not necessary for jump escape behaviors, provided that the second nerve cord remains intact, since the DIMD can presumably take over its role.

What Is the Effect of Selective Contralateral Ablation of the DCMD on Behavior?

Next, we selectively ablated the DCMD in one nerve cord by filling it intracellularly with 6-carboxy-fluorescein, a phototoxic dye, and shining laser light onto it (Experimental Procedures). In addition, we sectioned the other nerve cord. This allowed us to determine whether the DCMD is necessary among descending *contralateral* neurons for the generation of looming-evoked escape behaviors. Since other axons, including the DIMD receiving input from the ipsilateral eye, should remain intact in the spared nerve cord, we used stimulation of the ipsilateral eye as a control (Figure 8, inset).

We could successfully carry out the ablation procedure in 9 locusts (out of 40 locusts in which the procedure was attempted), as evidenced by the selective disappearance of the DCMD spikes from extracellular recordings in response to looming stimuli (Figures S6A and S6B and Laser Ablation Optical Setup). We could subsequently elicit jumps in four of these locusts. An additional five animals prepared for but did not carry out a jump in response to looming stimuli to either eye. Since these experiments were carried out without a telemetry backpack, we analyzed the jump preparation sequence in these nine locusts based on simultaneously acquired video recordings. The timing of the IJM (see Figures 1 and 3), which is a proxy for the activation onset of flexor motor neurons in intact animals (Fotowat and Gabbiani, 2007), did not differ when stimulating the eye ipsi- or contralateral to the remaining nerve cord. However, it showed higher variability in response to stimulation of the contralateral eye and a lower correlation with l/|v| (Figure 8; $\rho_{contra} = 0.48$, $p = 0.009$; $\rho_{ipsi} = 0.69$, $p < 10^{-9}$). Three out of the four locusts that jumped did so only in response to stimulation of the eye ipsilateral to the spared cord, but one jumped in response to stimulation of either eye. In this locust, the probability of jumping was slightly lower for contralateral eye stimulation ($n_{jump\text{-}ipsi} = 4$, $Prob_{jump\text{-}ipsi} = 33\%$, $n_{jump\text{-}contra} = 2$, $Prob_{jump\text{-}contra} = 20\%$). The two jumps in response to contralateral eye stimulation occurred 60 and 140 ms *after* projected collision, considerably later than observed in intact animals for l/|v| = 80 ms (mean: 68 ms *before* collision; SD = 42 ms; $n_L = 7$, $n_T = 89$). Indeed, in intact animals, in only two trials for one animal—2.2% of all trials— did take-off occur after collision, with the latest take-off time being 35 ms

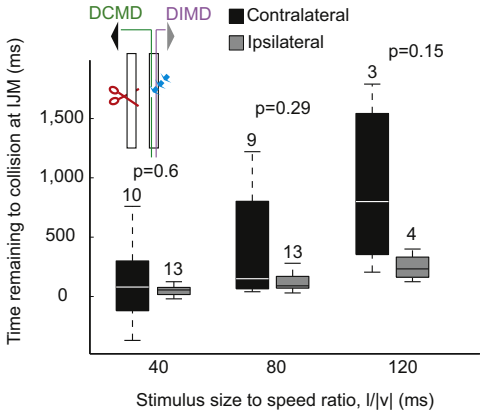

Figure 8. Effect of DCMD Laser Ablation on the Escape Behavior

The timing of the IJM (box plots), a proxy for the start of flexor motoneuron activity in intact animals, in response to looming stimuli presented to the eye contralateral to the ablated DCMD was not significantly different from control (i.e., when looming stimuli were presented to the eye ipsilateral to the intact nerve cord). See also Figure S6. The timing of IJM, however, showed more variability (coefficient of variation, CV_{ipsi} = 0.8, 0.5, 0.5 and CV_{contra} = 2.68, 1.16, 0.8, for l/|v| = 40, 80, and 120 ms, respectively). Inset: the ablation configuration with the left nerve cord sectioned (red scissors) and the DCMD laser ablated (blue arrows). Black and grey triangles indicate stimulated eyes; DIMD indicates the projection of the DIMD through the intact nerve cord.

after collision. In contrast, the two jumps elicited by ipsilateral stimulation at the same l/|v| value occurred 0 and 10 ms *before* collision, and were thus relatively close to the range observed in intact animals.

Since one locust jumped in response to stimulation of the eye contralateral to the nerve cord where we had ablated the DCMD, this indicates that other contralateral descending neurons respond to looming stimuli (as recently reported by Gray et al., 2010) and are able to activate the motor circuitry generating the jump. In fact, after all nine successful DCMD ablations, we could still record multiunit activity elicited by looming stimuli in the affected nerve cord (Figure S6B). The peak of the multiunit activity, however, occurred significantly later than that of the DCMD (106 ms, difference of medians; $p_{KWT} < 10^{-9}$). In three of the animals that jumped after DCMD laser ablation, including the one that jumped on both sides, we measured the activity of the nerve cord in response to looming stimuli presented to the eye ipsi and contralateral to the remaining nerve cord after the behavioral experiments (Figure S6C). The DIMD spikes were detectable as the largest in response to stimulation of the ipsilateral eye, while one or more unidentified units were activated in response to contralateral eye stimulation. We presented looming stimuli with nine different l/|v| values and compared the timing of the peak multiunit activity evoked in the contralateral nerve cord to the stimulated eye with that of the DIMD. We found that the peak multiunit activity occurred later than that of the DIMD (Figure S6D). Because the DCMD peak firing rate occurs earlier or around the time of the DIMD peak (Figure S5B), we conclude that for all l/|v| values, the peak multiunit contralateral activity occurs later than the DCMD peak.

These results indicate that, among contralateral descending neurons, the DCMD plays a critical role in the timely triggering of cocontraction and take-off but probably not in the generation of the initial hindleg flexion and joint movement. Furthermore, other descending contralateral units can trigger a jump, but given their delayed peak activity, these jumps occur close to, or even after expected collision. Such delayed jumps are rare in intact animals.

DISCUSSION

Using a miniature telemetry system, we were able to record simultaneously the sensory and motor activity contributing to the execution of a complex, multistage escape behavior in freely behaving animals. This allowed us to study how variability in the sensory response affects the final motor output on a trial-by-trial basis. Our results suggest that the DCMD neuron contributes to multiple aspects of the behavior through several distinct attributes of its time-varying firing rate. In addition, ablation experiments suggest that, together with the DIMD neuron, the DCMD is an important element of the circuitry mediating timely escape behaviors. We expect that miniature wireless telemetry will contribute to the study of sensorimotor integration during free behavior in other species as well.

Understanding how sensory stimuli are processed by the nervous system to generate complex behaviors in real time is a central goal of systems and computational neuroscience. In this context, the relatively compact nervous system of many invertebrates offers a unique opportunity to study the contribution of single sensory neurons to natural behavior, particularly when they can be reliably identified and the neural circuitry in which they are embedded is well described. Such is the case of the DCMD neuron, whose properties have been characterized for over forty years (Burrows, 1996), allowing us to investigate how its visual responses contribute to distinct motor phases of an ongoing behavior.

We found little evidence for an involvement of the DCMD in the initial preparatory movements leading to the jump, while it played an increasingly important role as collision became imminent. Thus, a DCMD firing rate threshold predicted 36% of the variance of cocontraction onset, suggesting that other neurons still play an important role at this stage. Indeed, both proprioceptive feedback and the C interneuron, that receives DCMD input, are expected to contribute to cocontraction onset (Burrows and Pflüger, 1988; Pearson and Robertson, 1981). After the start of cocontraction, we found a very strong correlation between the number of DCMD and extensor spikes (Figure 4C; Supplemental Text), with the FETi firing rate following faithfully that of the DCMD (Figure S2B). Thus, cocontraction onset appears to act as a *switch* that triggers this faithful transmission mode. In contrast, DCMD spikes have previously been thought incapable of generating spikes in the FETi motoneuron (Burrows and Rowell, 1973; Rogers et al., 2007). In those studies, the peak DCMD firing rate was, however, lower than the threshold we report for triggering cocontraction. The DCMD was more active in our experiments most likely because of: (1) increased arousal in freely behaving animals (Rowell, 1971b); (2) increased ambient temperature (Experimental Procedures); (3) preselection of locusts that responded readily to looming stimuli (typically one third of the animals). Additionally, the EPSPs from the DIMD

presumably summated with those of the DCMD (Burrows and Rowell, 1973), consistent with our finding that jump probability was reduced by 50% in locusts with one nerve cord sectioned.

The DIMD is thus an important confounding factor when studying the role of the DCMD in the generation of visually guided escape behaviors, as it conveys nearly identical information to motor centers about impending collision. The existence of this neuron and its similarity to the DCMD had been reported early on (Burrows and Rowell, 1973; Rowell, 1971). Yet, its responses to looming stimuli had not been recorded and its function has since been overlooked. In addition, the circuitry generating visually guided escape behaviors is remarkably robust since elimination of half of the information traveling from the brain to motor centers has little effect on their execution. Thus, assessing the role played by the DCMD with cell-specific laser ablation required simultaneous sectioning of the other nerve cord. These experiments are technically difficult and had a low success rate (4/40 = 10%). In three out of four animals, no jumps were elicited when stimuli were presented contralateral to the laser ablated DCMD. In the remaining one, jumps in response to stimulation of the contralateral eye occurred considerably later than to ipsilateral stimulation. This result is consistent with our finding that the peak activity in remaining contralateral looming sensitive units occurs significantly later as well (Figures S6C and S6D). We conclude that, among contralateral descending neurons, the DCMD is necessary for the accurate timing of the escape behavior. In zebrafish, selective laser ablation of the Mauthner array of neurons, also eliminates short-latency, high-performance escape responses but still leaves fish capable of generating a longer latency and slower escape response, presumably via other neural pathways (Liu and Fetcho, 1999).

We could predict 75% of the trial-to-trial variability of the jump time from the DCMD peak firing time. The time course of the decay in DCMD firing rate following its peak could contribute to it (Fotowat and Gabbiani, 2007). Other potential sources of variability include the DIMD, additional looming sensitive neurons, local interneurons, and sensory feedback (Pearson et al., 1980; Gynther and Pearson, 1989; Jellema and Heitler, 1999).

Finally, we found that the number of DCMD spikes from co-contraction onset was highly predictive of jump occurrence. A classifier trained with this attribute performed even better than one trained with the number of extensor spikes. This points to the fact that the DCMD activity controls jump execution not only through activation of the leg extensor motor neurons but also through other factors, such as the onset of flexor inhibition.

In conclusion, the transformation of sensory activity into the motor program leading to visually guided jumps appears to rely on at least three distinct attributes of a single neuron's time-varying discharge: a firing rate threshold, the peak firing rate time and the number of spikes from a specific time point (cocontraction onset). This multiplexing of motor-related information in a sensory neuron's response could not be evidenced in earlier experiments where behavior and electrophysiology were carried out separately (Fotowat and Gabbiani, 2007) or when animals were restrained to a trackball (Santer et al., 2008). Although our results strongly suggest multiplexing, they do not definitively prove it. This will require specific manipulation of the DCMD activity during ongoing behavior. Multiplexing of sensory information across populations of neurons has been documented earlier, particularly in the vertebrate visual and olfactory system, but its relation to behavior remains to be determined (Meister, 1996; Friedrich et al., 2004; for a review see Panzeri et al., 2010). In invertebrates, several examples of neurons that contribute to distinct, and sometimes mutually exclusive, motor behaviors have been studied as well. These neurons can be thought of as being multiplexed, but on a very different time scale as that evidenced here (Kristan and Shaw, 1997). Our finding that distinct aspects of a complex, time-dependent motor behavior can be encoded by distinct attributes of the time-varying firing rate of a single sensory neuron suggests that similar encoding may occur at the sensory-motor interface in other systems, including vertebrates.

EXPERIMENTAL PROCEDURES

Wireless Telemetry

We designed and built a custom integrated circuit that performs the amplification, analog to digital conversion, multiplexing, and wireless transmission of four low-noise channels: two for neural and two for muscle recordings (Figure S1). The neural and muscle recordings are amplified with gains of 1000 and 100, respectively, and filtered in the range of 300 Hz–5.2 kHz and 20 Hz–280 Hz, respectively. A 9 bit analog-to-digital converter samples them at 11.52 kHz and 1.92 kHz, respectively. The digital wireless transmitter operates based on a frequency-shift keying scheme at 920 MHz. The size of the packaged chip is 5×5 mm^2 and was mounted on a 13×9 mm^2 printed circuit board (PCB). Data from an accelerometer mounted on the PCB were also transmitted (ADXL330, Analog Devices, Norwood, MA; sampling rate: 1.92 kHz, bandwidth: 0–500 Hz). The accelerometer provided high temporal resolution but saturated for accelerations above $\sim 3.8\ g_n$ ($g_n = 9.8$ m/s^2). Therefore, we estimated the peak acceleration based on the video recordings. For this purpose, we tracked the position of the locust eye frame-by-frame and computed numerically its second derivative around the time of the peak. Wireless telemetry ran for 2 hr on a pair of 1.5 V batteries (#337, Energizer, St. Louis, MO). The weight of the system including batteries was 0.79 g (1.2 g after connecting and fixing the transmitter to the animal). The receiver captures the transmitted signals via a half-wavelength monopole antenna and relays them to a computer via a USB port through which it is also powered.

Animal Preparation for Wireless Telemetry

We used adult female locusts weighing more than 2.5 g. Locusts were fixed ventral side up on a holder and a rectangular window was cut open on the cuticle of their thorax. Teflon-coated Stablohm wires of 50 μm diameter were used for extracellular recordings (California Fine Wire, Grover Beach, CA). The coating was removed at the desired recording site. A hook-shaped electrode was implanted around one of the nerve cords between the pro- and mesothoracic ganglia, and the ground and reference electrodes were placed inside the thorax. The cuticle window was then closed and sealed with Vetbond (3M, St. Paul, MN) and beeswax. A pair of electrodes was inserted in the flexor and extensor muscles of the hindleg ipsilateral to the nerve implant and secured with Vetbond and beeswax. The extensor muscle was impaled dorsally from the outside in segment b, which is innervated by the FETi motorneuron (Hoyle, 1978). The flexor muscle was impaled medially. For each muscle, the reference electrode was inserted 1 mm from the recording electrode. The four muscle electrodes were bundled together inside a polyimide tube (085-1; MicroLumen, Tampa, FL) to minimize their movement and entanglement with the legs. The other end of the implanted electrodes was soldered to miniature connectors (0508 and 3061; Mill-Max, Oyster Bay, NY). The animal was then fixed dorsal side up with electric tape and the wireless transmitter system was attached to the cuticle around the neck with an equal mixture of rosin and beeswax. The connector ends of the electrodes were then soldered to the telemetry system inputs.

Looming Stimuli

Discs approaching on a collision course with the animal were simulated on a computer screen as described previously (Gabbiani et al., 1999; Fotowat and Gabbiani, 2007; monitor refresh rate = 200 fps). Briefly, the instantaneous angular size, $\theta(t)$, subtended at one eye by a disk of radius, l, approaching the animal at constant speed, v, is fully characterized by the ratio, $l/|v|$, since $\theta(t) = 2 \times \tan^{-1}(l/(v \times t))$. By convention, $v < 0$ for approaching stimuli and $t < 0$ before collision.

Video Recordings

A high-speed digital video camera (IPX-VGA210; Imperx, Boca Raton, FL), equipped with a zoom lens (LIM250M; Kowa, Torrance, CA) was used to record the escape behavior. Recordings were obtained at 100 frames per second with each frame acquisition triggered by alternate frames of the visual stimulation computer.

Behavior with Full Stimulus Expansion

The behavioral setup and conditions were identical to those described earlier (Fotowat and Gabbiani, 2007). Ten locusts equipped with the telemetry system were presented looming stimuli with $l/|v|$ = 40, 80, and 120 ms. These values correspond to the lower, middle, and upper part of the range eliciting reliable escape behaviors. In six locusts, one channel of nerve cord recording was transmitted. In the other four locusts, the activity of flexor and extensor muscles was also recorded.

Behavior with Partial Stimulus Expansion

Nine locusts were presented looming stimuli with $l/|v|$ = 40, 80, and 120 ms. The final radius was chosen randomly from 1, 1/2, 1/4, 1/8, and 1/16 of the full size. We identified the smallest final size at which the cocontraction was initiated and varied it slightly around that value to get a better estimate. Nerve cord, flexor, and extensor muscle activities were recorded and transmitted wirelessly as described above.

Simultaneous Recordings from Both Nerve Cords

The extracellular activity of the nerve cords ipsi- and contralateral to the stimulated eye was recorded simultaneously in nine fixed locusts at $l/|v|$ = 10–60 (in steps of 10), 80, 100, and 120 ms.

Nerve Cord Ablation Experiments

Looming-evoked escape behaviors were studied in six locusts, before and after cutting one of their nerve cords. Looming stimuli were presented to the eyes ipsi- and contralateral to the sectioned nerve cord at $l/|v|$ = 40, 80, and 120 ms.

Animal Preparation and Electrophysiology for Laser Ablation

Laser ablation allows the selective inactivation of a single neuron after filling it with a phototoxic dye (Miller and Selverston, 1979; Jacobs and Miller, 1985). Animals were mounted ventral side up on a holder, and a hook electrode was implanted around one nerve cord between the pro- and mesothoracic ganglia; the other nerve cord was sectioned, and the cuticle was sealed back in place. The quality of the extracellular nerve cord recording was then tested; laser ablation was only attempted when it was high (e.g., Figure S6A). Next, the locust head was tilted backward and a vertical incision was made in the neck skin, exposing the nerve cords running between the subesophageal and prothoracic ganglia. A small area of the intact nerve cord was desheathed with fine forceps. To achieve mechanical stability during intracellular recordings, we raised the nerve cord and secured it in place with a pair of polyimide tubes placed under and at the boundary of the desheathed area (039-1; MicroLumen, Tampa, FL). Glass electrodes were pulled on a Brown-Flaming micropipette puller (P-97, Sutter Instrument Company, Novato, CA) with thin-wall capillaries with an outer diameter of 1.2 mm (WPI, Sarasota, FL). The tips of the electrodes were filled with 4 μl of 10 mM 6-carboxy-fluorescein (Sigma, St. Louis, MO) and the shafts with 6 μl of a 2 M KAc, 0.5 M KCl solution. The electrode resistances varied between 45 and 50 MΩ. The DCMD axon is located dorsomedially in the nerve cord and was identified based on the one-to-one correspondence with the largest spikes in the extracellular recording. It was filled by electrophoresis for 12 min with currents between −1 and −12 nA. The filling was monitored visually by means of a fluorescence module attached to a stereomicroscope. After filling, the intracellular electrode was removed and the saline level was lowered to minimize the loss of laser power because of light scattering. Laser light was directed onto the axon while the activity of the DCMD was monitored on the extracellular electrode to confirm its eventual laser ablation, typically after 2–5 min.

Laser Ablation Optical Setup

We used a Cyan Scientific 488 nm, 20 mW, continuous wave laser (Spectra-Physics Laser Division, Newport, Santa Clara, CA). The beam was expanded ten times with two lenses arranged in a telescope configuration (LB1437-A and LB 1092-A, Thorlabs, Newton, NJ) and directed toward the nerve cord with two mirrors and a focusing lens (10D20DM.5, Newport, LBF254-100-A, Thorlabs).

Behavior and Electrophysiology after Laser Ablation

Because the laser ablation procedure involves a long sequence of technically challenging steps, the overall success rate was low. In fact, to date, in none of the studies that have used laser ablation for selective inactivation of insect neurons has the natural behavior of the animals been tested afterwards (Warzecha et al., 1993; Heitler, 1995; Farrow et al., 2003). In 17 out of 40 locusts in which the procedure was attempted we could successfully ablate the DCMD with minimal apparent damage to the nerve cord. Out of these 17 locusts, 9 reacted to looming stimuli when tested behaviorally, but only 4 jumped in response to them. In these four animals, the entire procedure most likely affected only the DCMD, as evidenced by subsequent behavior and electrophysiological recordings (Figure S6). Indeed, in three of these four animals, we recorded robust responses to looming stimuli from the remaining nerve cord several hours (and up to 3 days) after laser ablation. While we cannot exclude nonspecific damage in the five animals that prepared but did not jump to looming stimuli, their jump preparation was similar to that of the other four. Thus, pooled results of these nine animals are presented in Figure 8. In any case, any nonspecific damage in these animals would not affect our conclusions. Our results are consistent with previous reports that laser ablation is selective for the cell that is dye-filled (Miller and Selverston, 1979; Jacobs and Miller, 1985).

Data Analysis

Custom MATLAB software was used for data acquisition and analysis (Mathworks, Natick, MA). The DCMD and motor neuron spikes were detected by thresholding. Estimates of the DCMD and motor neurons' instantaneous firing rates were computed by convolving individual spike trains with a Gaussian function (width: 20 ms) as described earlier (Gabbiani et al., 1999). In some jump trials the nerve recording showed some distortions around the time of the peak firing rate (Supplemental Text and Figure S7). We estimated that we could have missed up to three consecutive DCMD spikes around that time. However, this incident did not significantly change the DCMD peak firing rate amplitude and time. The Kruskal-Wallis test (KWT) was used to compare the medians of populations across different treatments. When a significant difference was found, Tukey's honestly significant difference criterion was used to perform multiple comparisons between pairs of medians. In all box plots, the whiskers show the nonoutlier extent, + signs depict outliers, and the top and bottom of the box show the upper and lower quartiles of the data. The horizontal bar inside the box shows the median. Outliers are defined as points larger than $q_u + 1.5(q_u - q_l)$ or smaller than $q_l - 1.5(q_u - q_l)$, where q_u and q_l are the upper and lower quartiles of the data, respectively. Least square linear regression was used for all fits. The Pearson's correlation coefficient is denoted by ρ; associated significance values refer to the null hypothesis $\rho = 0$. Partial correlations (ρ_{part}) were calculated to estimate the correlation between two of three intercorrelated variables, controlling for the effect of the third. The percentage of variance of a variable explained by a second correlated variable was estimated as the square of their correlation coefficient. Naive Bayes classification was used to estimate the predictive power of different sensory and motor attributes for the trial outcome (jump versus no jump). The probability distributions of individual attributes (required for training the classifier) were estimated empirically and nonparametrically. An estimate of the misclassification rate (i.e., the rate of false positive or false negative

errors) for each classifier was obtained by training it on half of the data chosen from 100 random data shuffles and testing it on the other half. The performances of the classifiers trained on different attributes were then compared with the KWT with multiple comparisons.

SUPPLEMENTAL INFORMATION

Supplemental Information includes Supplemental Experimental Procedures, seven figures, and two movies and can be found with this article online at doi:10.1016/j.neuron.2010.12.007.

ACKNOWLEDGMENTS

This work was supported by the Air Force Research Laboratory, Human Fronteir Science Program, National Institute of Mental Health, and National Science Foundation. We would like to thank Drs. H. Krapp and J. Maunsell and Mr. P. Jones for comments.

Accepted: October 18, 2010
Published: January 12, 2011

REFERENCES

Burrows, M. (1996). The Neurobiology of an insect brain (Oxford: Oxford University Press).

Burrows, M., and Pflüger, H. (1988). Positive feedback loops from proprioceptors involved in leg movements of the locust. J. Comp. Physiol. A Neuroethol. Sens. Neural Behav. Physiol. *163*, 425–440.

Burrows, M., and Rowell, C.F. (1973). Connections between descending visual interneurons and metathoracic motoneurons in the locust. J. Comp. Physiol. *85*, 221–234.

Camhi, J.M., and Levy, A. (1989). The code for stimulus direction in a cell assembly in the cockroach. J. Comp. Physiol. A Neuroethol. Sens. Neural Behav. Physiol. *165*, 83–97.

Cohen, M.R., and Newsome, W.T. (2009). Estimates of the contribution of single neurons to perception depend on timescale and noise correlation. J. Neurosci. *29*, 6635–6648.

Cook, E.P., and Maunsell, J.H.R. (2002). Dynamics of neuronal responses in macaque mt and vip during motion detection. Nat. Neurosci. *5*, 985–994.

De Lafuente, V., and Romo, R. (2005). Neuronal correlates of subjective sensory experience. Nat. Neurosci. *8*, 1698–1703.

Edwards, D.H., Heitler, W.J., and Krasne, F.B. (1999). Fifty years of a command neuron: The neurobiology of escape behavior in the crayfish. Trends Neurosci. *22*, 153–161.

Farrow, K., Haag, J., and Borst, A. (2003). Input organization of multifunctional motion-sensitive neurons in the blowfly. J. Neurosci. *23*, 9805–9811.

Fotowat, H., and Gabbiani, F. (2007). Relationship between the phases of sensory and motor activity during a looming-evoked multistage escape behavior. J. Neurosci. *27*, 10047–10059.

Fotowat, H., Fayyazuddin, A., Bellen, H.J., and Gabbiani, F. (2009). A novel neuronal pathway for visually guided escape in drosophila melanogaster. J. Neurophysiol. *102*, 875–885.

Friedrich, R.W., Habermann, C.J., and Laurent, G. (2004). Multiplexing using synchrony in the zebrafish olfactory bulb. Nat. Neurosci. *7*, 862–871.

Gabbiani, F., Krapp, H.G., and Laurent, G. (1999). Computation of object approach by a wide-field, motion-sensitive neuron. J. Neurosci. *19*, 1122–1141.

Gabbiani, F., Mo, C., and Laurent, G. (2001). Invariance of angular threshold computation in a wide-field looming-sensitive neuron. J. Neurosci. *21*, 314–329.

Gabbiani, F., Krapp, H.G., Koch, C., and Laurent, G. (2002). Multiplicative computation in a visual neuron sensitive to looming. Nature *420*, 320–324.

Gabbiani, F., Cohen, I., and Laurent, G. (2005). Time-dependent activation of feed-forward inhibition in a looming-sensitive neuron. J. Neurophysiol. *94*, 2150–2161.

Gray, J.R., Blincow, E., and Robertson, R.M. (2010). A pair of motion-sensitive neurons in the locust encode approaches of a looming object. J. Comp. Physiol. A Neuroethol. Sens. Neural Behav. Physiol. 10.1007/s00359-010-0576-7.

Graziano, M.S., Andersen, R., and Snowden, R. (1994). Tuning of mst neurons to spiral motions. J. Neurosci. *14*, 54–67.

Gu, Y., Angelaki, D.E., and Deangelis, G.C. (2008). Neural correlates of multisensory cue integration in macaque MSTd. Nat. Neurosci. *11*, 1201–1210.

Gynther, I.C., and Pearson, K.G. (1989). An evaluation of the role of identified interneurons in triggering kicks and jumps in the locust. J. Neurophysiol. *61*, 45–57.

Hatsopoulos, N., Gabbiani, F., and Laurent, G. (1995). Elementary computation of object approach by wide-field visual neuron. Science *270*, 1000–1003.

Heitler, W.J. (1995). Quasi-reversible photo-axotomy used to investigate the role of extensor muscle tension in controlling the kick motor programme of grasshoppers. Eur. J. Neurosci. *7*, 981–992.

Hoyle, G. (1978). Distributions of nerve and muscle fibre types in locust jumping muscle. J. Exp. Biol. *73*, 205–233.

Ishikane, H., Gangi, M., Honda, S., and Tachibana, M. (2005). Synchronized retinal oscillations encode essential information for escape behavior in frogs. Nat. Neurosci. *8*, 1087–1095.

Jacobs, G.A., and Miller, J.P. (1985). Functional properties of individual neuronal branches isolated in situ by laser photoinactivation. Science *228*, 344–346.

Jellema, T., and Heitler, W.J. (1999). Central and peripheral control of the trigger mechanism for kicking and jumping in the locust. J. Comp. Neurol. *404*, 212–220.

Judge, S., and Rind, F.C. (1997). The locust dcmd, a movement-detecting neurone tightly tuned to collision trajectories. J. Exp. Biol. *200*, 2209–2216.

Killmann, F., and Schurmann, F. (1985). Both electrical and chemical transmission between the 'lobula giant movement detector' and the 'descending contralateral movement detector' neurons of locusts are supported by electron microscopy. J. Neurocytol. *14*, 637–652.

Korn, H., and Faber, D.S. (2005). The mauthner cell half a century later: A neurobiological model for decision-making? Neuron *47*, 13–28.

Kristan, W.B., and Shaw, B.K. (1997). Population coding and behavioral choice. Curr. Opin. Neurobiol. *7*, 826–831.

Lewis, J.E., and Kristan, W.B., Jr. (1998). A neuronal network for computing population vectors in the leech. Nature *391*, 76–79.

Lima, S.Q., and Miesenböck, G. (2005). Remote control of behavior through genetically targeted photostimulation of neurons. Cell *121*, 141–152.

Liu, K.S., and Fetcho, J.R. (1999). Laser ablations reveal functional relationships of segmental hindbrain neurons in zebrafish. Neuron *23*, 325–335.

Marsat, G., and Pollack, G.S. (2006). A behavioral role for feature detection by sensory bursts. J. Neurosci. *26*, 10542–10547.

Meister, M. (1996). Multineuronal codes in retinal signaling. Proc. Natl. Acad. Sci. USA *93*, 609–614.

Miller, J.P., and Selverston, A. (1979). Rapid killing of single neurons by irradiation of intracellularly injected dye. Science *206*, 702–704.

Mountcastle, V.B., Lynch, J.C., Georgopoulos, A., Sakata, H., and Acuna, C. (1975). Posterior parietal association cortex of the monkey: Command functions for operations within extrapersonal space. J. Neurophysiol. *38*, 871–908.

Nakagawa, H., and Hongjian, K. (2010). Collision-sensitive neurons in the optic tectum of the bullfrog, Rana catesbeiana. J. Neurophysiol. *104*, 2487–2499.

Newsome, W.T., Wurtz, R.H., and Komatsu, H. (1988). Relation of cortical areas MT and MST to pursuit eye movements. ii. differentiation of retinal from extraretinal inputs. J. Neurophysiol. *60*, 604–620.

Nienborg, H., and Cumming, B.G. (2009). Decision-related activity in sensory neurons reflects more than a neuron's causal effect. Nature *459*, 89–92.

O'Shea, M., Rowell, C., and Williams, J. (1974). The anatomy of a locust visual interneurone; the descending contralateral movement detector. J. Exp. Biol. *60*, 1–12.

Oliva, D., Medan, V., and Tomsic, D. (2007). Escape behavior and neuronal responses to looming stimuli in the crab chasmagnathus granulatus (decapoda: Grapsidae). J. Exp. Biol. *210*, 865–880.

Panzeri, S., Brunel, N., Logothetis, N.K., and Kayser, C. (2010). Sensory neural codes using multiplexed temporal scales. Trends Neurosci. *33*, 111–120.

Pearson, K., and Robertson, R. (1981). Interneurons coactivating hindleg flexor and extensor motoneurons in the locust. J. Comp. Physiol. A Neuroethol. Sens. Neural Behav. Physiol. *144*, 391–410.

Pearson, K.G., Heitler, W.J., and Steeves, J.D. (1980). Triggering of locust jump by multimodal inhibitory interneurons. J. Neurophysiol. *43*, 257–278.

Peron, S., and Gabbiani, F. (2009). Spike frequency adaptation mediates looming stimulus selectivity in a collision-detecting neuron. Nat. Neurosci. *12*, 318–326.

Preuss, T., Osei-Bonsu, P.E., Weiss, S.A., Wang, C., and Faber, D.S. (2006). Neural representation of object approach in a decision-making motor circuit. J. Neurosci. *26*, 3454–3464.

Rind, F.C. (1984). A chemical synapse between two motion detecting neurones in the locust brain. J. Exp. Biol. *110*, 143–167.

Rind, F.C., and Simmons, P. (1992). Orthopteran dcmd neuron: A reevaluation of responses to moving objects. I. selective responses to approaching objects. J. Neurophysiol. *68*, 1654–1666.

Rogers, S.M., Krapp, H.G., Burrows, M., and Matheson, T. (2007). Compensatory plasticity at an identified synapse tunes a visuomotor pathway. J. Neurosci. *27*, 4621–4633.

Roitman, J.D., and Shadlen, M.N. (2002). Response of neurons in the lateral intraparietal area during a combined visual discrimination reaction time task. J. Neurosci. *22*, 9475–9489.

Rowell, C. (1971). The orthopteran descending movement detector (dmd) neurones: A characterisation and review. J. Comp. Physiol. A Neuroethol. Sens. Neural Behav. Physiol. *73*, 167–194.

Rowell, C. (1971b). Variable responsiveness of a visual interneurone in the free-moving locust, and its relation to behaviour and arousal. J. Exp. Biol. *55*, 727–747.

Santer, R.D., Yamawaki, Y., Rind, F.C., and Simmons, P.J. (2005). Motor activity and trajectory control during escape jumping in the locust Locusta migratoria. J. Comp. Physiol. A Neuroethol. Sens. Neural Behav. Physiol. *191*, 965–975.

Santer, R.D., Rind, F.C., Stafford, R., and Simmons, P. (2006). Role of an identified looming-sensitive neuron in triggering a flying locust's escape. J. Neurophysiol. *95*, 3391–3400.

Santer, R.D., Yamawaki, Y., Rind, F.C., and Simmons, P.J. (2008). Preparing for escape: An examination of the role of the dcmd neuron in locust escape jumps. J. Comp. Physiol. A Neuroethol. Sens. Neural Behav. Physiol. *194*, 69–77.

Schlotterer, G.R. (1977). Response of the locust descending movement detector neuron to rapidly approaching and withdrawing visual stimuli. Can. J. Zool. *55*, 1372–1376.

Simmons, P. (1980). Connexions between a movement-detecting visual interneurone and flight motoneurones of a locust. J. Exp. Biol. *86*, 87–97.

Sun, H., and Frost, B. (1998). Computation of different optical variables of looming objects in pigeon nucleus rotundus neurons. Nat. Neurosci. *1*, 296–303.

Trimarchi, J.R., and Schneiderman, A.M. (1993). Giant fiber activation of an intrinsic muscle in the mesothoracic leg of drosophila melanogaster. J. Exp. Biol. *177*, 149–167.

van Hateren, J.H., Kern, R., Schwerdtfeger, G., and Egelhaaf, M. (2005). Function and coding in the blowfly H1 neuron during naturalistic optic flow. J. Neurosci. *25*, 4343–4352.

Wang, Y., and Frost, B.J. (1992). Time to collision is signaled by neurons in the nucleus rotundus of pigeons. Nature *356*, 236–238.

Warzecha, A.K., Egelhaaf, M., and Borst, A. (1993). Neural circuit tuning fly visual interneurons to motion of small objects. I. Dissection of the circuit by pharmacological and photoinactivation techniques. J. Neurophysiol. *69*, 329–339.

Wicklein, M., and Strausfeld, N.J. (2000). Organization and significance of neurons that detect change of visual depth in the hawk moth manduca sexta. J. Comp. Neurol. *424*, 356–376.

Yamamoto, K., Nakata, M., and Nakagawa, H. (2003). Input and output characteristics of collision avoidance behavior in the frog rana catesbeiana. Brain Behav. Evol. *62*, 201–211.